ELSEVIER

Contents lists available at ScienceDirect

Journal of Alloys and Compounds

journal homepage: www.elsevier.com/locate/jalcom



Effects of intrinsic defects on electronic structure and optical properties of Ga-doped ZnO



Ming-Hsien Lee a, Yen-Chun Peng b, Hsuan-Chung Wu b,*

- ^a Department of Physics, Tamkang University, New Taipei 25137, Taiwan
- ^b Department of Materials Engineering, Ming Chi University of Technology, New Taipei 24301, Taiwan

ARTICLE INFO

Article history:
Received 14 April 2014
Received in revised form 23 June 2014
Accepted 13 July 2014
Available online 19 July 2014

Keywords: Ab initio ZnO Intrinsic defects Electronic structure Optical properties

ABSTRACT

This study adopted ab initio methods to calculate the effects of intrinsic defects on the electrical and optical properties of Ga-doped ZnO (GZO). The defective types of GZO considered in this study include O vacancies ($Ga_{Zn}V_O$), Zn vacancies ($Ga_{Zn}V_{Zn}$), interstitial O ($Ga_{Zn}O_i$), and a non-defective type (Ga_{Zn}). The results for calculating formation energy show that, during the GZO preparation process, the growth environment influences the type of intrinsic defects that occur. Under poor O conditions, a $Ga_{Zn}V_O$ structure is most likely to form; conversely, under rich O conditions, $Ga_{Zn}V_{Zn}$ or $Ga_{Zn}O_i$ is most likely to form. The calculated results regarding band structure and density of states indicate that the V_O defect present in the $Ga_{Zn}V_O$ model produces a deep donor level, which substantially reduces transmittance. The V_{Zn} and O_i defects in $Ga_{Zn}V_{Zn}$ or $Ga_{Zn}O_i$ models reduce carrier concentration and mobility. Subsequently, reduced carrier concentration and mobility significantly increase resistivity. The Ga_{Zn} structure can be fabricated by introducing appropriate O flow rates during the preparation process. This structure possesses superior photoelectric features. The results obtained in this study were compared with previous experimental literature to explain the potential reasons for the shift in electrical and optical properties under varying O flow rates.

© 2014 Elsevier B.V. All rights reserved.

1. Introduction

Tin-doped In₂O₃ (ITO) is currently the most common choice of transparent conductive oxides (TCOs) because it features low resistivity and high transmittance properties. However, the In used in ITO is environmentally toxic and expensive, which consequently increases manufacturing costs [1–3]; thus, in recent years, numerous studies have been conducted to reduce the In content of products, or to locate alternative substitutes. ZnO is a wide band gap semiconductor (3.37 eV) and displays transparent properties in visible light. In addition, Zn is abundantly available in the earth and non-toxic [4]. Consequently, ZnO has been widely researched to determine its suitability for manufacturing TCOs and has been widely used in other photoelectric applications, such as solar cells [5], light emitting devices [6], transistors [7], and diluted magnetic semiconductors [8].

The resistivity of pure ZnO is of the $10^{-2}\,\Omega$ cm order, which is far greater than that of ITO ($10^{-4}\,\Omega$ cm order). To enhance conduc-

E-mail address: hcwu@mail.mcut.edu.tw (H.-C. Wu).

tivity, ZnO is typically doped with additional elements. Dopants can primarily be divided into metal [9-13] and non-metal [14,15] elements. The ionic radii of Ga³⁺ (0.62 Å) and Zn²⁺ (0.74 Å) are similar [16]. This facilitates extremely low structural strain after doping and increases solubility. In addition, numerous studies have developed Ga-doped ZnO (GZO) with a resistivity of the $10^{-4} \,\Omega$ cm order. Therefore, GZO is a potential substitute for ITO when manufacturing TCOs. The photoelectric features of GZO are associated not only with doping concentration, but also preparation methods and process parameters. Numerous studies [17-22] have comprehensively investigated the effects that process parameters (i.e., oxygen flow rate, sputtering power, and substrate temperature) have on the electrical and optical properties of GZO, endeavoring to determine optimal TCO performance. Yamada et al. [17] investigated the effects that various Ga_2O_3 contents and O flow rates have on the electrical properties of GZO films. Their findings indicated that a minimum resistivity of $2.23 \times 10^{-4} \,\Omega$ cm was obtained with a 4 wt% doping concentration and 2.5 SCCM O. After the O flow rate reached the threshold of 2.5 SCCM, the resistivity of the films increased significantly with subsequent increases in the O flow rate. Sato et al. [18] showed that the resistivity of GZO initially decreases and then increases following the gradual increase of the O flow rate from 5 to 25 SCCM, contending that the intrinsic

^{*} Corresponding author. Address: Department of Materials Engineering, Ming Chi University of Technology, 84 Gungjuan Road, Taishan, New Taipei 24301, Taiwan. Tel.: +886 2 29089899x4675: fax: +886 2 29084091.

defects affect GZO resistivity. This implies that various O flow rates influence the quantity and form of intrinsic defects, which consequently influences the electrical properties of GZO. The connection between O₂ flow rate and the optical absorption spectra of GZO films has been studied by the same group [19]. They indicated that an increase in O₂ flow rate during the deposition would decrease the intensity of the free carrier absorption and the absorption band between 2 eV and 3 eV and shift the fundamental optical gap absorption to a long wavelength. Osada et al. [20] indicated that O vacancy (V_0) occurs easily when O flow is not introduced during the GZO film preparation process. After introducing up to 10 SCCM of O flow rate, V_0 content shows reduction tendencies. When the O flow rate exceeds 10 SCCM, excess O exists in the process environment and compensating defects, such as interstitial $O(O_i)$ atoms or Zn vacancies (V_{Zn}) , form easily, which consequently results in increased resistivity. Several other studies [21,22] have indicated that these compensating defects increase transmittance: however. they also decrease carrier concentration and mobility.

Based on these discussions, different process conditions affect the type and quantity of intrinsic defects, which consequently influences the electrical and optical properties of GZO; that is, the correlations among process, structure, and property. To fully understand the photoelectric features of GZO, it is necessary to conduct in-depth investigations on the effects that intrinsic defects have on the electrical and optical properties of GZO. Theoretical calculations provide information regarding material microscopic view to further understand the correlation between structure and property. In our prior study, the density functional theory plus Hubbard U (DFT + U) method was used to resolve band gap underestimations when using standard DFT. The deviations of the calculated band gap and lattice constants when using this method are both within 1% of the experimental values [23]. This study further extended the application of this method to calculate and analyze the effects that various intrinsic defects (i.e., V_0 , V_{Zn} , and O_i) have on the formation energy, electronic structure, and optical properties of GZO, simultaneously comparing the obtained results with other experiment-based literature. These results clarify the correlations among the process, structure, and properties of GZO and can be used to set criteria for future material designs.

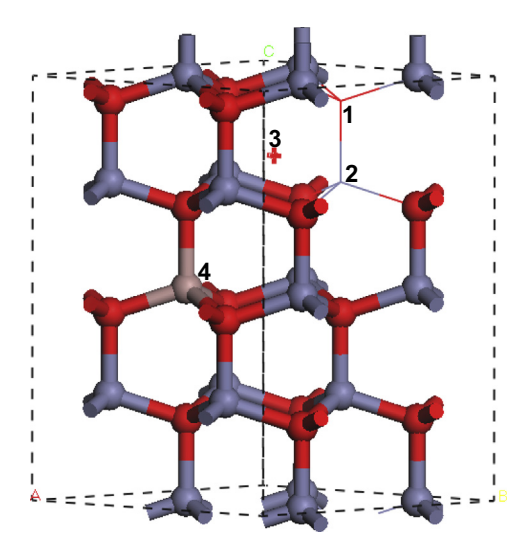


Fig. 1. A $2 \times 2 \times 2$ ZnO supercell, where the red components represent the O atoms, gray represents the Zn atoms, and Numbers 1 to 4 respectively represent the V_O , V_{Zn} , O_i , and Ga replacements for Zn. (For interpretation of the references to color in this figure legend, the reader is referred to the web version of this article.)

2. Calculation models and methods

This study considered a $2 \times 2 \times 2$ ZnO supercell, containing 16 Zn atoms and 16 O atoms, as shown in Fig. 1. Numbers 1 to 4 respectively represent O vacancies (V_O) , Zn vacancies (V_{Zn}) , interstitial O (O_i) , and Ga substitutions for Zn (Ga_{Zn}) . In cases where Ga_{Zn} simultaneously contains other intrinsic defects, these complex defects manifest as $Ga_{Zn}V_O$, $Ga_{Zn}V_{Zn}$, and $Ga_{Zn}O_i$. The replacement or removal of one Zn or O atom would result in a defect concentration of approximately 6 at.% (1/16). The defect concentration could be reduced using a larger supercell; however, this study was limited with regard to computer resources. A $2 \times 2 \times 2$ ZnO supercell such as this has been adopted in numerous previous studies to calculate the properties of ZnO with intrinsic defects [24–26].

All models investigated in this study were calculated using the CASTEP [27] software package. Structural optimization was performed on each model prior to calculating their electrical and optical properties. Software settings were as follows: the plane wave cutoff energy was set at 380 eV; a $4 \times 4 \times 2$ Monkhorst-Pack grid was used to set the k-point sampling [28]; energy convergence criterion for the self-consistent field was set at 10^{-6} eV; the ultrasoft pseudopotential method [29] was used to calculate the ion core, and the valence electrons for Zn, O, and Ga were set at 4s²3d¹⁰, 2s²2p⁴, and 4s²3d¹⁰4p¹, respectively. For structural optimization, the convergence criteria for energy, maximum force, maximum stress, and maximum displacement were set at 10^{-5} eV/atom, 3×10^{-3} eV/Å, 5×10^{-2} GPa, and 10^{-3} Å, respectively. To more accurately describe the exchange and correlation potential, this study adopted the DFT + U_d + U_p calculation method [30]. In this study, the $U_{\rm d}$ value for Zn-3d and the $U_{\rm p}$ value for O-2p orbitals were set at 10 and 7 eV, respectively. The calculated band gap and lattice constants were within a 1% mean error margin compared to the experimental values. The band structures, Zn-3d orbital locations, and ZnO band gaps used to select various U_d and U_p values can be referenced from our prior research [23,31].

3. Results and discussion

3.1. Types of intrinsic defects

This study analyzed the relative stability of GZO systems containing intrinsic defects based on formation energy, and simultaneously calculated the formation energy of individual intrinsic defects in ZnO for comparison. Formation energy of the various models in neutral charge state can be computed as [32,33]

$$E_{f}(D) = E_{tot}(D) - E_{tot}(ZnO) + \sum n_{i}\mu_{i}$$
(1)

where $E_{\rm tot}$ (ZnO) and $E_{\rm tot}$ (D) separately represent the total energy for pure ZnO and the defective systems. $n_{\rm i}$ is the number of atom i added to or removed from the supercell. If the atom is added to the supercell, $n_{\rm i}$ is negative, otherwise is positive. $\mu_{\rm i}$ represents the chemical potential of the various atoms. Formation energy is influenced by the growth environment during the experimental preparation process. Increased O flow rate is regarded as an O-rich condition; conversely, poorly ventilated O or decreased O flow rate is regarded as an O-poor condition. In thermo-dynamic equilibrium, $\Delta\mu_{\rm Zn} + \Delta\mu_{\rm O} = \Delta H_{\rm f}$ (ZnO), where $\Delta H_{\rm f}$ (ZnO) is the formation enthalpy of ZnO. $\Delta\mu_i$ is the chemical potential of atom i referenced to its elemental solid/gas of $\mu_{\rm i(bulk)}$. The chemical potentials are calculated as follows:

$$\mu_{Zn} = \mu_{Zn(bulk)} + \Delta H_f(ZnO), \mu_O = \mu_{O(O_2)}(O\text{-rich conditions})$$
 (2)

$$\mu_{\text{Zn}} = \mu_{\text{Zn(bulk)}}, \mu_{\text{O}} = \mu_{\text{O(O}_2)} + \Delta H_f(\text{ZnO})(\text{O-poor conditions})$$
 (3)

The chemical potential of Ga is taken as the energy of bulk metallic Ga.

The calculated chemical potentials are μ_{Zn} = -4.65 eV, μ_{O} = -4.35 eV and μ_{Ga} = -2.70 eV (O-rich conditions); μ_{Zn} = -1.16 eV, μ_{O} = -7.84 eV and μ_{Ga} = -2.70 eV (O-poor conditions). The formation energy calculated for each type of defective system based on the neutral charge state is shown in Table 1. Lower formation energy denotes an increased occurrence of defects. Based on the calculated results, the following main points are provided:

Table 1 Formation energy for ZnO and GZO with varying intrinsic defects.

Formation energy (eV)	V_{O}	$V_{\rm Zn}$	O_i	Ga_{Zn}	$Ga_{Zn}V_O$	$Ga_{Zn}V_{Zn}$	$Ga_{Zn}O_i$
O-rich condition	4.33	3.09	3.95	−3.70	0.27	-2.89	-1.53
O-poor condition	0.84	6.58	7.44	−0.21	0.27	4.10	5.46

- 1. For a single intrinsic defect in ZnO, $E_f(V_{zn}) < E_f(O_i) < E_f(V_O)$ under O-rich conditions. This implies that O-rich conditions were most prone to induce V_{Zn} , followed by O_i and V_O . Under O-poor conditions, $E_f(V_O) < E_f(V_{Zn}) < E_f(O_i)$. This implies that O-poor conditions were most prone to induce V_O ; V_{Zn} and O_i were not easily formed.
- 2. With the presence of Ga_{Zn} , the order of difficulty for the formation of intrinsic defects was similar to that of ZnO. That is, the order of facility for the formation of intrinsic defects $V_{Zn} > O_i > V_O$ for O-rich conditions, and $V_O > V_{Zn} > O_i$ for O-poor conditions.
- The presence of Ga_{Zn} were comparatively more likely to induce intrinsic defects than pure ZnO.

3.2. Electrical properties

The formation energy mentioned in Section 3.1 indicates that O flow rate influences the occurrence and form of intrinsic defects in GZO during the preparation process. The occurrence of $Ga_{Zn}V_O$ was most probable with a low-O flow rate (i.e., O-poor conditions), and $Ga_{Zn}V_{Zn}$ and $Ga_{Zn}O_i$ were most likely to occur with a high-O flow rate (i.e., O-rich conditions). The experimental resistivity, carrier concentration, and transmittance trends in GZO following increases in O flow rate are shown in Fig. 2 [20-22]. Fig. 3(a)-(d) shows the band structures corresponding to the 4 defective types. This was used to explain the electrical properties for different O flow rates under experimental conditions. Fig. 4 shows the density of states of the 4 defective types. The Fermi energy shown in Figs. 3 and 4 was set at the 0 eV position. Fig. 3(a) shows the band structure of GaZn in moderate O flow rate conditions. When the Zn atoms in pure ZnO were substituted by Ga, the Fermi level shifted from the valence band maximum to the bottom of the conduction band. This resulted in a shallow donor level at the bottom of the conduction band, producing n-type conduction features. This shallow donor level was primarily contributed by the Ga-4s and Ga-4p orbitals, as shown in Fig. 4(a). In addition, the optical band gap increased to 4.72 eV (from pure ZnO to Ga_{Zn}).

At low O flow rates, the defective state $Ga_{Zn}V_O$ was most likely to occur. The occurrence of V_O in GZO expanded the optical band gap to 5.37 eV and caused the formation of a deep donor level in

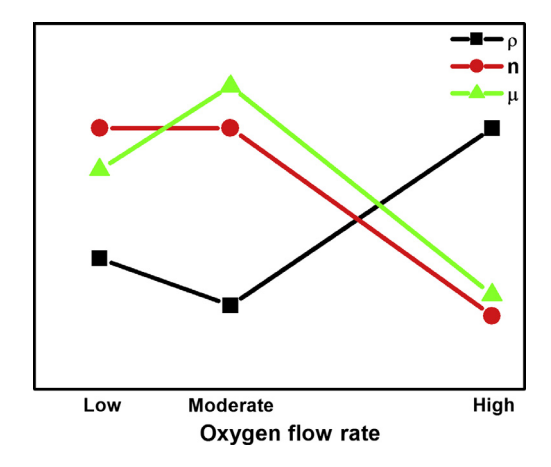


Fig. 2. Relationship between O flow rate and the resistivity (ρ) , carrier concentration (n), and mobility (μ) of GZO [15–17].

the band gap (Fig. 3(b)). Because deep donor levels do not significantly contribute to increasing carrier concentrations, the carrier concentration of $Ga_{Zn}V_O$ was similar to that of Ga_{Zn} . In the band structure, the curvature closer to the bottom of the conduction band influenced the size of the electron effective mass. A larger curvature denotes a smaller effective mass, which facilitated an increase in the electron mobility. Comparing Fig. 3(a) and (b) indicates that the presence of V_O caused a decreased curvature at the bottom of the conduction band, which consequently decreased the mobility. Therefore, increasing the O flow rate from low to moderate effectively increases mobility, consequently reducing the resistivity of GZO [9,17,21]. Fig. 4(b) shows that the deep donor level in the band gap caused by V_O was contributed by the O-2p orbital, which significantly reduced the transmittance of GZO.

At high O flow rates, V_{Zn} and O_i were easily formed in GZO. The band structures for the $Ga_{Zn}V_{Zn}$ and $Ga_{Zn}O_i$ models are shown in Fig. 3(c) and (d), which are comparatively similar. In addition, both the V_{Zn} and O_i defects caused the O-2p orbitals of the O atoms close to the defects to form unoccupied states and, because O inherently possesses greater electronegativity, charge compensation centers are more likely to form. When donor (Ga_{Zn}) and acceptor (V_{Zn}) or O_i) levels coexist, the unoccupied states produced by V_{Zn} or O_i seize the electrons of the Ga_{Zn} donor level, thereby causing the Fermi level to decline to the top of the valence band. Although the band gaps for $Ga_{Zn}V_{Zn}$ and $Ga_{Zn}O_i$ can be narrowed to 3.00 and 2.88 eV, respectively, the generation of free electrons necessitates more energy to be stimulated from the valence band to the conduction band compared to the GaZn model. This causes carrier concentration to rapidly decline. In addition, based on Fig. 4(c) and (d), the $Ga_{Zn}V_{Zn}$ and $Ga_{Zn}O_i$ models form a more localized energy state between approximately 4 and 6 eV, which corresponds to the energy band with the small curvature in the conduction band shown in Fig. 3(c) and (d). This implies that the effective mass expanded and reduced mobility. Therefore, when V_{Zn} or O_i defects are present in GZO, these defects reduce both carrier concentration and mobility, which consequently increases the resistivity of GZO at high O flow rates [9].

According to [34], the addition of 1.4×10^{21} cm⁻³ Ga donors to ZnO would result in the formation of 1.7×10^{20} cm⁻³ Zn-vacancy acceptors in the lattice with a ratio of Ga_{Zn} to V_{Zn} of approximately 8:1. The order of facility in the formation of intrinsic defects is $V_{Zn} > O_i$ under O-rich as well as O-poor conditions, which implies that the ratio of Ga_{Zn} to O_i exceeds 8:1. Thus, in practical cases, the doped Ga donors should not be fully compensated by V_{Zn} and O_i and the Fermi level would be within the bottom of the conduction band (n-type conduction). However, the unoccupied O-2p states produced by V_{Zn} or O_i seize the partial electrons at the Ga_{Zn} donor level, resulting in a decline in the Fermi level and carrier concentration below that found in the Ga_{Zn} model.

3.3. Optical properties

Fig. 5 shows the absorption spectrum of GZO with varying intrinsic defects. In contrast to ZnO, blueshift of the intrinsic absorption edge occurred in both the Ga_{Zn} and $Ga_{Zn}V_O$ models because of increased optical band gaps, and shallow donor levels resulted in absorption near the long-wavelength infrared region.

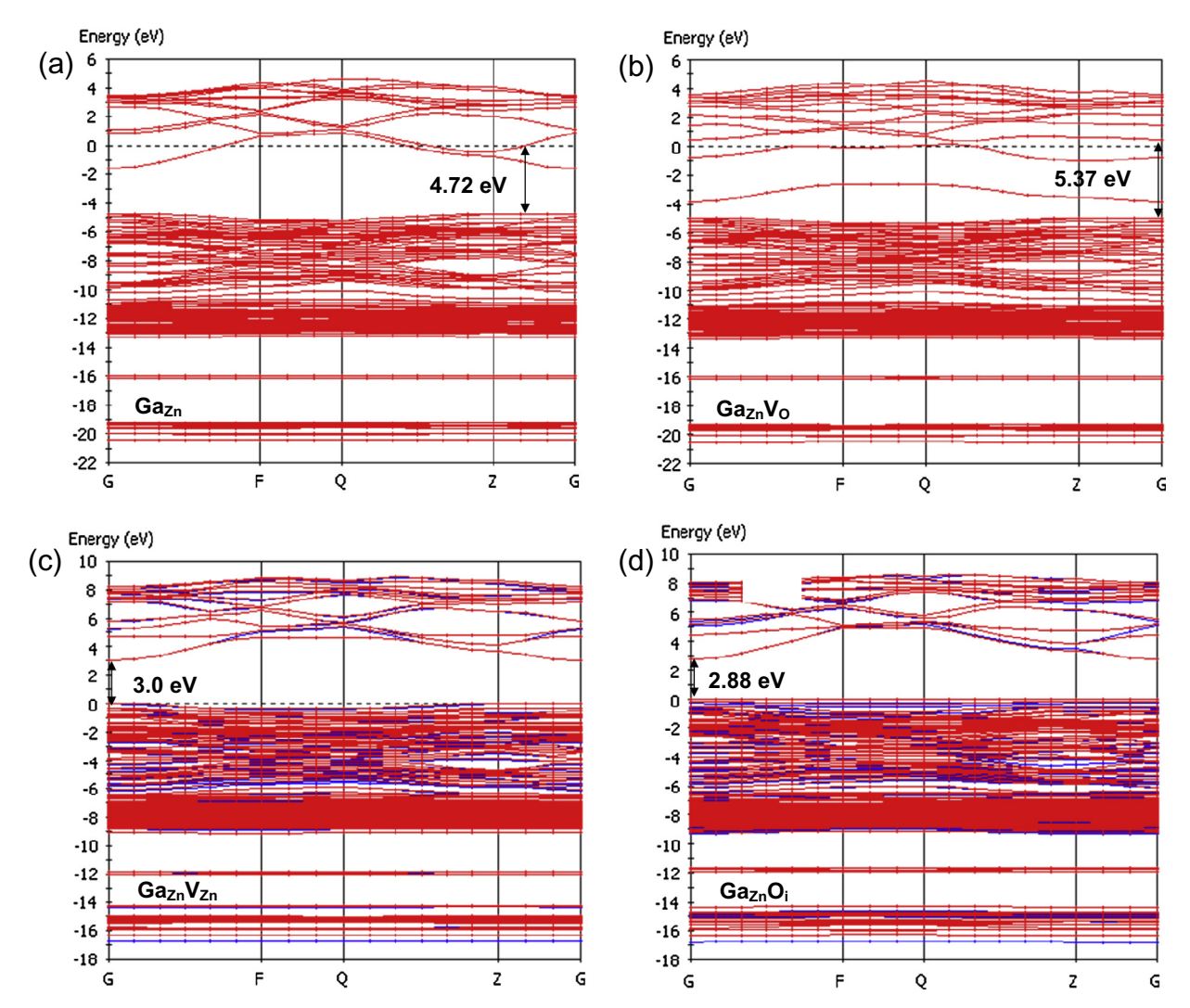


Fig. 3. Band structures of Ga-doped ZnO for (a) Ga_{Zn} , (b) $Ga_{Zn}V_O$, (c) $Ga_{Zn}V_{Zn}$, and (d) $Ga_{Zn}O_i$ models.

The order of intensity in the long-wavelength infrared region was shown to be $Ga_{Zn}V_O > Ga_{Zn} > Ga_{Zn}V_{Zn}/Ga_{Zn}O_i$, which is consistent with experimental results [19], where the intensity of the free carrier absorption decreased with an increase in O₂ flow rate. In Section 3.2, the deep donor level in the band gap of the $Ga_{Zn}V_{O}$ enhanced absorption in the range of approximately 500 nm to the ultraviolet region, which significantly decreased transmittance in the visible and UV regions. This is consistent with the experimental results in [19], in which GZO films deficient in oxygen were shown to be absorptive in the visible wavelength range. No occupied states were produced in the band gaps of the $Ga_{Zn}V_{Zn}$ and $Ga_{Zn}O_i$ models, and no absorption occurred under visible light. In contrast to the Ga_{Zn} model, V_{Zn} and O_i did not induce shallow donor levels, thereby eliminating the absorption of red/infrared light. In addition, the reduction of band gaps also caused the intrinsic absorption edge to shift towards the long wavelengths.

This study adopted the absorption coefficient, reflection coefficient, and film thickness to calculate transmittance. The equation is as follows:

$$T = (1 - R)^2 e^{-\alpha d} \tag{4}$$

where T represents transmittance, α and R respectively represent the absorption and reflection coefficients, and d represents the film thickness. In this study, d was set at 250 nm.

Fig. 6 shows the transmittance of the various defective GZO models. The results showed that, regardless of visible or ultraviolet light, the GaZnVO model demonstrated the lowest transmittance. Subsequently, when a suitable O flow rate was introduced to the Ga_{Zn}V_O model, V_O was eliminated to achieve a Ga_{Zn} structure. This significantly increased the transmittance of the model; particularly in visible light. The increase in transmittance was achieved primarily by eliminating the deep donor level. In addition, transmittance in ultraviolet light was also increased. $Ga_{Zn}V_{Zn}$ and $Ga_{Zn}O_i$ structures were further achieved by introducing larger quantities of O. Following the elimination of the shallow donor level, the transmittance increased when the wavelength was greater than 800 nm. However, because the optical band gap was reduced, the intrinsic absorption edge shifted to 400 nm, which consequently reduced the transmittance in ultraviolet light. To summarize Sections 3-2 and 3-3, the formation of the Ga_{Zn} model under appropriate quantities of O shows superior electrical and optical performance. Conversely, the formation of the $Ga_{Zn}V_O$ model under low O flow rates shows poor electrical and optical properties. The formation of the Ga_{Zn}V_{Zn} and Ga_{Zn}O_i models under high O flow rates demonstrated a transmittance capacity similar to ZnO. However, the formation of V_{Zn} or O_i decreased carrier concentration and mobility, which consequently increased resistivity.

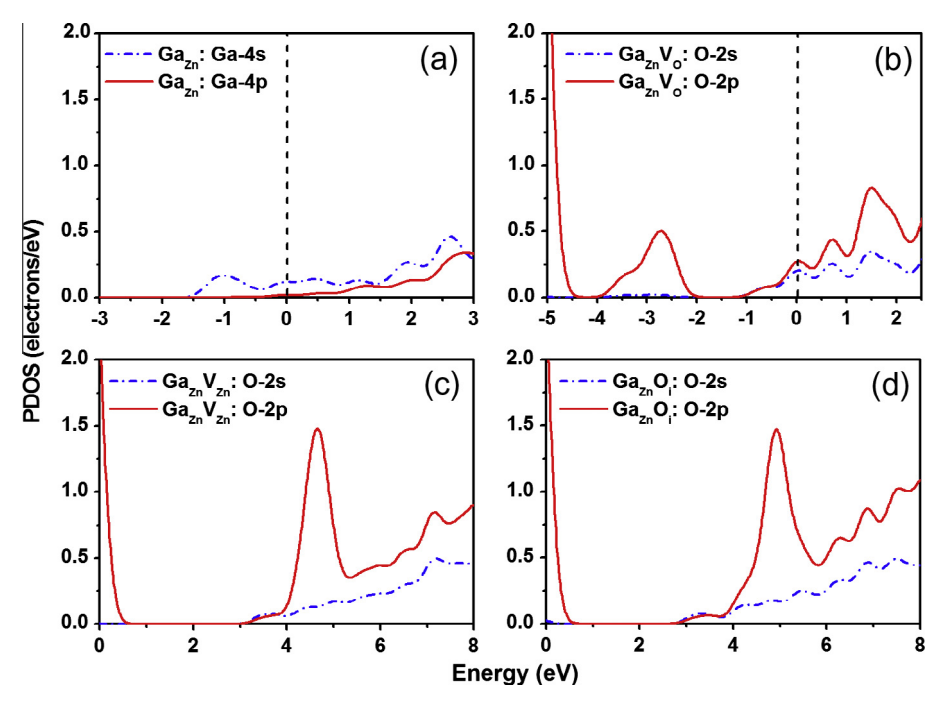


Fig. 4. Density of states for GZO with various intrinsic defects: (a) $Ga_{Zn}V_O$, (b) $Ga_{Zn}V_O$, (c) $Ga_{Zn}V_{Zn}$, and (d) $Ga_{Zn}O_i$.

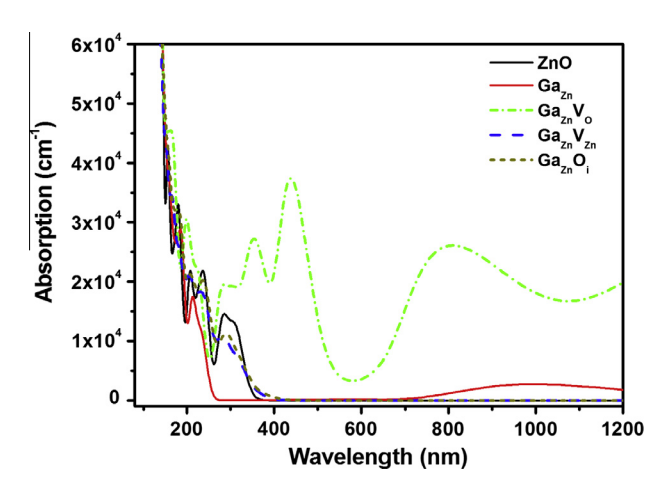


Fig. 5. Absorption coefficients of GZO with varying intrinsic defects.

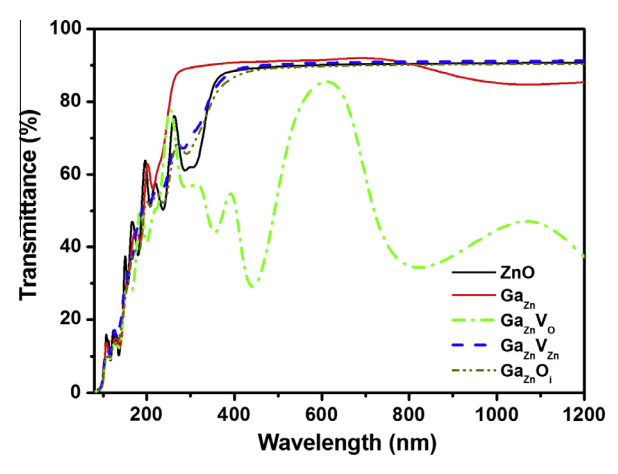


Fig. 6. Transmittance of GZO with varying intrinsic defects.

4. Conclusions

This study adopted the DFT + U_d + U_p method to calculate the formation energy, electronic structure, and optical properties of GZO with intrinsic defects. The calculated results of formation energy indicated that, regardless of ZnO or GZO, Vo was more likely to form than V_{Zn} and O_i under O-poor conditions, and $V_{\rm Zn}$ and O_i were more likely to form than $V_{\rm O}$ under O-rich conditions. Thus, when preparing GZO with low, moderate, and high O flow rates, the most probable structures derived would be (in order) $Ga_{Zn}V_O$, Ga_{Zn} and $Ga_{Zn}V_{Zn}$ or $Ga_{Zn}O_i$. The $Ga_{Zn}V_O$ model suggested that the deep donor level produced by V_0 does not facilitate the increase of carrier concentration, and significantly reduces transmittance. When introducing moderate amounts of O, Vo can be eliminated to produce a Gazn model, which consequently eliminates the formation of deep donor levels. This increases the curvature of the energy band at the bottom of the conduction band and increases carrier mobility, which consequently reduces resistivity and significantly increases the transmittance under visible and ultraviolet light. However, excess O content may induce the formation of the $Ga_{Zn}V_{Zn}$ or $Ga_{Zn}O_i$ models. $V_{\rm Zn}$ and O_i eliminate the shallow donor level provided by Ga, which reduces carrier concentrations. In addition, these two defects cause a flatter acceptor level in the conduction band and reduce mobility. Subsequently, the reduced carrier concentrations and mobility significantly decrease conductivity. Therefore, considering the performance of TCO, the formation of the Ga_{Zn} structure under appropriate O flow rates demonstrates superior photoelectric features.

Acknowledgements

This work was supported by the National Science Council in Taiwan (NSC 102-2221-E-131 -008), for which the authors are grateful. We also acknowledge the National Center for Highperformance Computing for computer time and the use of its facilities.

References

- [1] D. Xu, Z. Deng, Y. Xu, J. Xiao, C. Liang, Z. Pei, C. Sun, An anode with aluminum doped on zinc oxide thin films for organic light emitting devices, Phys. Lett. A 346 (2005) 148–152.
- [2] M. Omura, A. Tanaka, M. Hirata, N. Inoue, T. Ueno, T. Homma, K. Sekizawa, Testicular toxicity evaluation of indium-tin oxide, J. Occup. Health 44 (2002)
- [3] J. Owen, M.S. Son, K.H. Yoo, B.D. Ahn, S.Y. Lee, Organic photovoltaic devices with Ga-doped ZnO electrode, Appl. Phys. Lett. 90 (2007) 033512.
- [4] I.L. Zhao, X.W. Sun, H. Ryu, Y.B. Moon, Thermally stable transparent conducting and highly infrared reflective Ga-doped ZnO thin films by metal organic chemical vapor deposition, Opt. Mater. 33 (2011) 768-772.
- [5] Z. Zang, A. Nakamura, J. Temmyo, Single cuprous oxide films synthesized by radical oxidation at low temperature for PV application, Opt. Express 21 (2013) 11448.
- [6] H.H. Huang, S.Y. Chu, P.C. Kao, Y.C. Chen, M.R. Yang, Z.L. Tseng, Enhancement of hole-injection and power efficiency of organic light emitting devices using an ultra-thin ZnO buffer layer, J. Alloys Comp. 479 (2009) 520–524. [7] J.F. Wager, Transparent electronics, Science 300 (2003) 1245–1246.
- [8] K. Wu, S. Gu, K. Tang, J. Ye, S. Zhu, M. Zhou, Y. Huang, M. Xu, R. Zhang, Y. Zheng, Temperature-dependent magnetization in (Mn, N)-codoped ZnO-based diluted magnetic semiconductors, J. Magn. Magn. Mater. 324 (2012) 1649-1654.
- [9] L.M. Wong, S.Y. Chiam, J.Q. Huang, S.J. Wang, W.K. Chim, J.S. Pan, Examining the transparency of gallium-doped zinc oxide for photovoltaic applications, Sol. Energy Mater. Sol. Cells 95 (2011) 2400-2406.
- [10] Y. Geng, L. Guo, S.S. Xu, Q.Q. Sun, S.J. Ding, H.L. Lu, D.W. Zhang, Influence of Al doping on the properties of ZnO thin films grown by atomic layer deposition, J. Phys. Chem. C 115 (2011) 12317–12321.
- [11] C. Huang, M. Wang, Z. Deng, Y. Cao, Q. Liu, Z. Huang, Y. Liu, W. Guo, Q. Huang, Effects of hydrogen annealing on the structural, optical and electrical properties of indium-doped zinc oxide films, J. Mater. Sci.: Mater. Electron. 21 (2010) 1221–1227.
- [12] H.P. Chang, F.H. Wang, J.C. Chao, C.C. Huang, H.W. Liu, Effects of thickness and annealing on the properties of Ti-doped ZnO films by radio frequency magnetron sputtering, Curr. Appl. Phys. 11 (2011) S185-S190.
- [13] V. Gokulakrishnan, S. Parthiban, K. Jeganathan, K. Ramamurthi, Investigation on the effect of Zr doping in ZnO thin films by spray pyrolysis, Appl. Surf. Sci. 257 (2011) 9068-9072.
- [14] L. Gao, Y. Zhang, J.M. Zhang, K.W. Xu, Boron doped ZnO thin films fabricated by RF-magnetron sputtering, Appl. Surf. Sci. 257 (2011) 2498–2502.
- J. Clatot, G. Campet, A. Zeinert, C. Labrugère, M. Nistor, A. Rougier, Low temperature Si doped ZnO thin films for transparent conducting oxides, Sol. Energy Mater. Sol. Cells 95 (2011) 2357-2362.
- [16] C.Y. Tsay, K.S. Fan, C.M. Lei, Synthesis and characterization of sol-gel derived gallium-doped zinc oxide thin films, J. Alloys Comp. 512 (2012) 216-222.
- [17] T. Yamada, K. Ikeda, S. Kishimoto, H. Makino, T. Yamamoto, Effects of oxygen partial pressure on doping properties of Ga-doped ZnO films prepared by ionplating with traveling substrate, Surf. Coat. Technol. 201 (2006) 4004-4007.

- [18] Y. Sato, H. Makino, N. Yamamoto, T. Yamamoto, Structural, electrical and moisture resistance properties of Ga-doped ZnO films, Thin Solid Films 520 (2011) 1395-1399.
- [19] H. Makino, T. Yamada, N. Yamamoto, T. Yamamoto, Effects of the O2 flow rate and post-deposition thermal annealing on the optical absorption spectra of Ga-doped ZnO films, Thin Solid Films 519 (2010) 1521-1524.
- [20] M. Osada, T. Sakemi, T. Yamamoto, The effects of oxygen partial pressure on local structural properties for Ga-doped ZnO thin films, Thin Solid Films 494 (2006) 38-41.
- [21] S. Kim, W.I. Lee, E.H. Lee, S.K. Hwang, C. Lee, Dependence of the resistivity and the transmittance of sputter-deposited Ga-doped ZnO films on oxygen partial pressure and sputtering temperature, J. Mater. Sci. 42 (2007) 4845-4849.
- [22] R.C. Scoot, K.D. Leedy, B. Bayraktaroglu, D.C. Look, Y.H. Zhang, Effects of Ar vs. O2 ambient on pulsed-laser-deposited Ga-doped ZnO, J. Cryst. Growth 324 (2011) 110-114.
- [23] H.C. Wu, Y.C. Peng, C.C. Chen, Effects of Ga concentration on electronic and optical properties of Ga-doped ZnO from first principles calculations, Opt. Mater. 35 (2013) 509-515.
- [24] J.H. Luo, Q. Liu, L.N. Yang, Z.Z. Sun, Z.S. Li, First-principles study of electronic structure and optical properties of (Zr-Al)-codoped ZnO, Comput. Mater. Sci. 82 (2014) 70-75.
- [25] Q.B. Wang, C. Zhou, J. Wu, T. Lü, A GGA + U study of the optical properties of vanadium doped ZnO with and without single intrinsic vacancy, Opt. Commun. 297 (2013) 79-84.
- [26] Y.F. Chen, Q.G. Song, H.Y. Yan, The electronic structures and magnetic properties of N-doped ZnO with and without Zn vacancy, Comput. Theor. Chem. 983 (2012) 65-68.
- [27] M.D. Segall, P.J.D. Lindan, M.J. Probert, C.J. Pickard, P.J. Hasnip, S.J. Clark, M.C. Payne, First-principles simulation: ideas, illustrations and the CASTEP code, J. Phys.: Condens. Matter 14 (2002) 2717-2744.
- [28] H.J. Monkhost, J.D. Pack, Special points for Brillouin-zone integrations, Phys. Rev. B 13 (1976) 5188-5192.
- [29] D. Vanderbilt, Soft self-consistent pseudopotentials in a generalized eigenvalue formalism, Phys. Rev. B 41 (1990) 7892-7895.
- [30] X. Ma, B. Lu, D. Li, R. Shi, C. Pan, Y. Zhu, Origin of photocatalytic activation of silver orthophosphate from first-principles, J. Phys. Chem. C 115 (2011) 4680-
- [31] H.C. Wu, Y.C. Peng, T.P. Shen, Electronic and optical properties of substitutional and interstitial Si-doped ZnO, Materials 5 (2012) 2088-2100.
- [32] A. Janotti, C.G. Van de Walle, Native point defects in ZnO, Phys. Rev. B: Condens. Matter 76 (2007) 165202.
- [33] T. Guo, G. Dong, Q. Chen, X. Diao, F. Gao, First-principles calculation on p-type conduction of (Sb, N) codoping in ZnO, J. Phys. Chem. Solids 75 (2014) 42-47.
- [34] D.C. Look, K.D. Leedy, L. Vines, B.G. Svensson, A. Zubiaga, F. Tuomisto, D.R. Doutt, L.J. Brillson, Self-compensation in semiconductors: the Zn vacancy in Ga-doped ZnO, Phys. Rev. B: Condens. Matter 84 (2011) 115202.